Allosteric Control of Ligand Selectivity between Estrogen Receptors α and β: Implications for Other Nuclear Receptors

ARTICLE *in* MOLECULAR CELL · MARCH 2004

Impact Factor: 14.02 · DOI: 10.1016/S1097-2765(04)00054-1 · Source: PubMed

8 AUTHORS, INCLUDING:

James T Radek
University of Wisconsin–Madison
22 PUBLICATIONS **816** CITATIONS
SEE PROFILE

Alice L Rodriguez
Vanderbilt University
54 PUBLICATIONS **1,795** CITATIONS
SEE PROFILE

John A Katzenellenbogen
University of Illinois, Urbana-Champaign
510 PUBLICATIONS **21,456** CITATIONS
SEE PROFILE

Geoffrey L Greene
University of Chicago
205 PUBLICATIONS **18,537** CITATIONS
SEE PROFILE

Molecular Cell, Vol. 13, 317–327, February 13, 2004, Copyright ©2004 by Cell Press

Allosteric Control of Ligand Selectivity between Estrogen Receptors α and β: Implications for Other Nuclear Receptors

Kendall W. Nettles,[1,4] Jun Sun,[2,4]
James T. Radek,[1] Shubin Sheng,[2]
Alice L. Rodriguez,[3] John A. Katzenellenbogen,[3]
Benita S. Katzenellenbogen,[2]
and Geoffrey L. Greene[1,*]
[1]Ben May Institute for Cancer Research
University of Chicago
Chicago, Illinois 60637
[2]Department of Molecular and
Integrative Physiology
[3]Department of Chemistry
University of Illinois
Urbana, Illinois 61801

Summary

Allosteric communication between interacting molecules is fundamental to signal transduction and many other cellular processes. To better understand the relationship between nuclear receptor (NR) ligand positioning and the formation of the coactivator binding pocket, we investigated the determinants of ligand selectivity between the two estrogen receptor subtypes ERα and ERβ. Chimeric receptors and structurally guided amino acid substitutions were used to demonstrate that distinct "hot spot" amino acids are required for ligand selectivity. Residues within the ligand binding pocket as well as distal secondary structural interactions contribute to subtype-specific positioning of the ligand and transcriptional output. Examination of other NRs suggests a mechanism of communication between the ligand and coactivator binding pockets, accounting for partial agonist and dimer-specific activity. These results demonstrate the importance of long-range interactions in the transmission of information through the ligand binding domain as well as in determining the ligand selectivity of closely related NR receptor subtypes.

Introduction

Nuclear receptors are allosteric transcription factors that engage in complex functional interactions with ligand, DNA, and transcriptional cofactor proteins, including coactivators and corepressors. The most carboxy-terminal helix (H12) of the nuclear receptor ligand binding domain (LBD) acts as a molecular switch, whose position determines the transcriptional readout of the receptor. In the agonist-bound structure, H12 forms one side of a hydrophobic coactivator binding pocket, or cleft, by docking against H3 and H11 in a highly conserved conformation (Supplemental Movie S1 at http://www.molecule.org/cgi/content/full/13/3/317/DC1). Transcriptional coactivator proteins (e.g., those of the p160 family) interact with nuclear receptors via LXXLL amino acid motifs that bind in this cleft, also known as the AF2 domain (Darimont et al., 1998; Nolte et al., 1998; Shiau et al., 2000). In contrast, the bulky side chains of antagonists, like tamoxifen and raloxifene, sterically block H12 from assuming an agonist position (Shiau et al., 1998), thereby preventing formation of the coactivator binding pocket and instead allowing H12 itself to dock in the hydrophobic cleft. Thus, H12 provides allosteric control of transcription from AF2 through its dynamic localization (Schulman et al., 1996).

The structural events underlying ligand-specific coactivator recruitment and transcriptional activation remain poorly understood for the NR superfamily. The development of ER subtype-selective ligands (Gaido et al., 1999; Meyers et al., 1999; Stauffer et al., 2000; Sun et al., 1999, 2003a) provides a molecular tool to study unresolved issues in the structural linkage between ligand and transcription. For example, there is no direct correlation between ligand affinity and transcriptional potency. Thus, while both ER subtypes have near identical affinities for estradiol, ERα demonstrates a greater potency in cell-based assays. There is also little structural information to explain the reduced efficacy seen with high-affinity partial agonist ligands, such as genistein. Ligand effects depend upon dimer partner for NRs that function as obligate dimers with the rexinoid X receptor (RXR) (DiRenzo et al., 1997). Current models suggest that the dynamics of H12 positioning are involved in these effects (Kallenberger et al., 2003; Love et al., 2002; Pike et al., 1999; Steinmetz et al., 2001; Webb et al., 2003), but the structural basis for the cooperative coupling between specific ligands and coactivators remains elusive.

To better understand the relationship between ligand positioning and transcriptional activation, we examined several ER subtype-selective ligands (Figure 1A) with different behaviors. THC (Meyers et al., 1999; Sun et al., 1999) and HPTE (Gaido et al., 1999, 2000) act as partial agonists on ERα but as full antagonists on ERβ, whereas PPT is an ERα-selective agonist (Stauffer et al., 2000; Sun et al., 1999). We examined both the structural inputs into ER-ligand positioning and how this positioning mediates ligand-specific transcriptional responses. Structure-based point mutations and ER subtype chimera were used to identify key amino acids that regulate ligand position and transcriptional output. We show that the critical determinants of ligand selectivity between ERα and ERβ vary with ligand structure. In some cases, selectivity results from proximal ligand-amino acid contacts inside the ligand binding pocket, whereas in other cases, selectivity derives from sequence differences outside the pocket. For THC, H11 controls the positioning of H12 into agonist or antagonist conformations, suggesting that H11 may play a wider role in nuclear receptor signaling.

This hypothesis was further evaluated by surveying ER, peroxisome-proliferator-activated receptor (PPAR), and RXR crystal structures for associations between ligand type, dimer type, and H11 conformation. H11 is differentially positioned in partial agonist versus full ago-

*Correspondence: ggreene@uchicago.edu
[4]These authors contributed equally to this work.

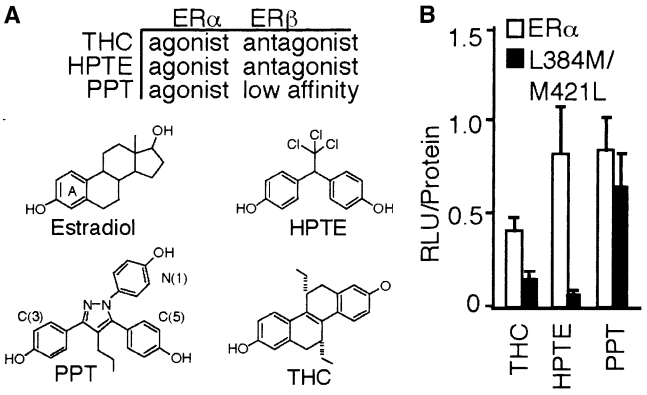

Figure 1. Estrogen Receptor Ligands and Effects on ERα

(A) Estradiol, HPTE [2,2-bis(p-hydroxyphenyl)-1,1,1-trichloroethane], PPT [propylpyrazoletriol, 1,3,5-tris(4-hydroxyphenyl)-4-propylpyrazole], and R,R-THC (5R,11R-diethyl-5,6,11,12-tetrahydrochrysene-2,8-diol) (THC).

(B) Ishikawa cells were transfected with ERα plasmids and an estrogen-responsive luciferase reporter, treated with the indicated ligands at 1 μM, and processed for luciferase activity.

nist crystal structures and in homodimer versus heterodimer structures of RXR and PPAR. Understanding these long-range contributions to allosteric function has important implications for the development of targeted therapeutics for the NR superfamily and for understanding basic principles underlying specificity in signal transduction.

Results

Ligand Binding Pocket Residues Account for ER Subtype Selectivity for HPTE but Not PPT or THC

To determine the basis of ligand selectivity for the ER subtypes, we first mutated residues within the ligand binding pockets of the two ERs, starting with the only two residues that differ between ERα and ERβ, Leu-384/Met-336 and Met-421/Ile-373 (Figure 1B, all mutations are summarized in Figure 2). HPTE activity was completely abrogated, THC activity was significantly reduced, and while there was no effect on the maximal efficacy of PPT (Figure 1B), the potency of PPT was reduced (data not shown). The ligand-specific effects of these mutations indicate that there are different structural contributions to the subtype specificity of the ligands, since THC and HPTE have similar activity profiles on wild-type ERα and ERβ.

Analysis of ERα/ERβ Chimeras

To evaluate the contributions of regions outside the ligand binding pocket, we used a more general screening approach. ERα and ERβ LBD chimeras were generated by PCR-mediated DNA shuffling, according to a protocol we have recently reported (Sun et al., 2003a, 2003b), and the activities of PPT and THC were then evaluated. The original screen for gain-of-function chimera was performed in yeast (data not shown) and then verified in mammalian cells. The chimeras studied have single, double, and sometimes multiple ERα/ERβ crossovers (Figures 3 and 4). We adopted a simple nomenclature system to describe these chimeras; the crossover sites

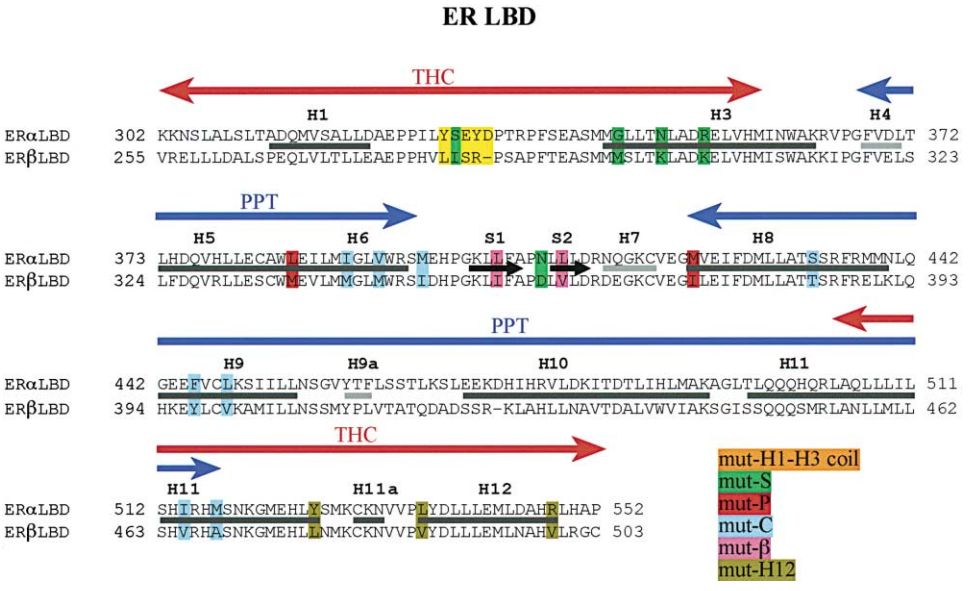

Figure 2. Sequence, Activity, and Mutagenesis Map of the Ligand Binding Domains of ERα and ERβ

The secondary structural elements in the LBD (helices and β sheets) are shown between the two sequences. The principal ERα activity-determining regions of PPT (hatched line) and THC (open line) are indicated, and sites where ERα residues have been substituted into the ERβ LBD sequence by mutagenesis are designated by color coding.

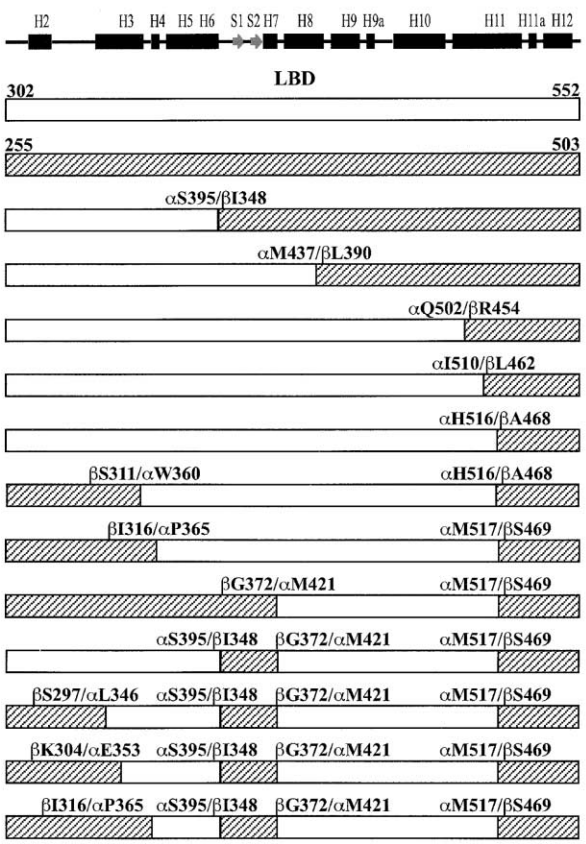

	Transactivation with 10^{-6} M PPT (% of 10^{-8} M E_2 on ERβ/αLBD)	Transactivation with 10^{-8} M E_2
ERα	120 ± 6	[100]
ERβ	0	79 ± 6
#1	0	99 ± 5
#2	30 ± 3	75 ± 3
#3	130 ± 6	60 ± 8
#4	110 ± 10	95 ± 8
#5	86 ± 6	85 ± 8
#6	98 ± 10	82 ± 9
#7	95 ± 11	76 ± 8
#8	5 ± 1	79 ± 10
#9	70 ± 3	65 ± 6
#10	68 ± 8	64 ± 6
#11	80 ± 15	63 ± 8
#12	95 ± 5	60 ± 9

Figure 3. Schematic Representations of ERα and ERβ Chimeric LBD Constructs and Activity of PPT

The secondary structure of the LBD is shown schematically at the top, with H representing a helix in the LBD and S a β strand. (Helices 9a and 11a are not consistently seen in the structures of both ERs.) The LBD sequences from ERα and ERβ are designated by open and hatched boxes, respectively. Each chimeric construct is also numbered (right), and the site of each crossover is specified by the residue numbers at the junction. These LBDs (domain E) were inserted into ERβ containing domains A–D and F. Maximal transactivation responses of the chimeras were determined at 10^{-6} M PPT, representing the mean ± SEM from three or more separate experiments. They are expressed as a percent of the response of the construct having a full ERα LBD to 10^{-8} M E2, set at 100% (right). The maximum activity of each chimera to 10^{-8} M E2 is also given (rightmost column).

from ERα to ERβ sequences or the reverse are designated as α[residue letter]###/β[residue letter]### or β[residue letter]###/α[residue letter]###, respectively. Chimeras are also numbered for easier reference.

ERα Selectivity for PPT

The chimera analysis demonstrates that a substantial portion of the ERα LBD is required for full PPT efficacy (Figure 3). We introduced the various ERα/β LBD chimeras into an ER having the β context in these other domains (A–D and F). In this manner, we could examine the extent of activity recovery for PPT that is obtained as progressively larger ERα LBD sequences are introduced into the ERβ context. When ERα sequences were progressively introduced into the N terminus of the ERβ LBD (chimeras 1–5), we found that PPT activity rises, reaching 30% as the ERα sequence reached the end of helix 8 (chimera 2) (Figure 3). Maximal activity levels were obtained, however, only when the ERα sequence extended to the start of H11 (chimeras 3–5). Interestingly, differences between ERα and ERβ in the distal C-terminal region of the LBDs, which includes H12, clearly known to be important for transactivation, are apparently not responsible for the ERα subtype-selective character of PPT.

To further define the minimal ERα sequence required for full PPT activity, we examined other chimeras in which ERβ sequences were introduced progressively into the N terminus of chimeras otherwise having ERα sequences through the start of H11 (chimeras 6–8). PPT maintained full efficacy until ERβ sequences reached beyond H4. Further analysis of PPT efficacy on ER chimeras having three or four crossovers (chimeras 8–12) allowed us to further localize the PPT activity-supporting ERα sequences to H4-6 and H8-10. Thus, by chimera analysis, full PPT efficacy required two segments of ERα sequences near the middle of the ER LBD, spanning helices 4–6 and H8 through the middle of H11. This portion of the LBD includes sequence elements that comprise one sector of the ligand binding pocket (H5-6), as well as elements that are quite distal to this pocket. Curiously, although PPT regains full efficacy on many of the ERα/β chimeras, for a number of these, PPT potency was reduced such that the dose-response curve was shifted approximately 10-fold to the right (data not shown). ERβ sequences that were responsible for this

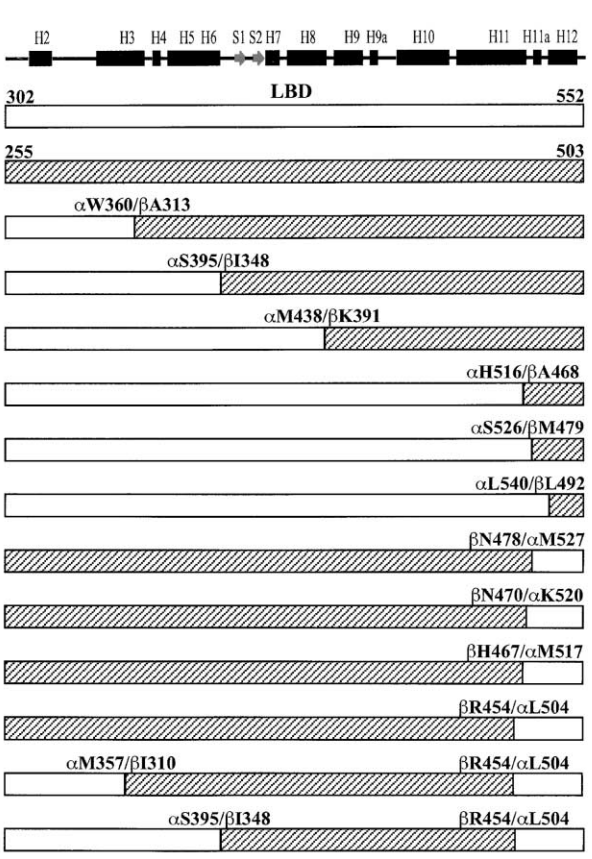

	Transactivation with 10^{-6} M R,R-THC (% of 10^{-8} M E_2 on ERα/αLBD)	Transactivation with 10^{-8} M E_2
ERα	50 ± 3	[100]
ERβ	6 ± 1	123 ± 13
#1	14 ± 2	91 ± 10
#2	23 ± 7	70 ± 10
#3	12 ± 3	87 ± 10
#4	19 ± 2	110 ± 14
#5	36 ± 3	119 ± 22
#6	44 ± 2	104 ± 8
#7	7 ± 1	134 ± 5
#8	12 ± 2	126 ± 17
#9	22 ± 3	159 ± 13
#10	32 ± 2	156 ± 20
#11	39 ± 2	113 ± 13
#12	49 ± 3	80 ± 7

Figure 4. Schematic Representations of ERα and ERβ Chimeric LBD Constructs and Activity of THC

The chimeric LBDs are depicted as in Figure 3 but were inserted into ERα containing domains A–D and F. Maximal transactivation responses of the chimeras were determined at 10^{-6} M THC. They are expressed as a percent of the response of the construct having a full ERα LBD to 10^{-8} M E2, set at 100% (right). The maximum activity of each chimera to 10^{-8} M E2 is also given (rightmost column).

PPT potency shift are in H3 of the LBD, outside the H4-6 region required for full efficacy. The segments contributing to PPT selectivity, which constitute about half of the LBD, are shown schematically in Figure 2.

Structural Basis of ER Subtype Selectivity for THC Is Distinct from PPT or HPTE

We performed a similar analysis of THC activity on a different set of ERα/β LBD chimeras having the α context in the other ER domains (A–D and F), through which THC works best. Although THC binds better to ERβ than to ERα (Meyers et al., 1999), it is a partial agonist on ERα (reaching an efficacy level of ca. 50%) and a complete antagonist in ERβ. For each chimera, the maximal activities obtained at saturating concentrations of THC, as well as that with 10^{-8} M estradiol, are listed in Figure 4.

Analysis of THC activity on chimeras in which ERα sequences were introduced progressively into the N terminus of the ERβ LBD shows that full to nearly full activity required ERα sequences to extend through the middle of H11 (chimeras 5 and 6), with lower efficacies being seen with shorter ERα LBD inserts. By contrast, analysis of complementary chimeras in which ERα sequences were introduced from the C terminus of the LBD showed that THC agonist activity quickly increased over a short sequence region (chimeras 7–10), reaching half to two-thirds of maximal, when ERα sequences encompassing only helices 11 and 12 were introduced (chimera 10). Further extension of ERα sequences did not reliably result in an increase of THC agonism (data not shown). Thus, it appears that sequences at both ends of the ERα LBD are required for maximal agonism of THC (Figure 2).

This hypothesis was tested by assessing THC activity on chimeras in which ERα sequence was introduced progressively from the N terminus into chimera 10 (in which helices 11 and 12 are already ERα). Nearly full activity was obtained when ERβ sequence through the beginning of H3 was replaced with ERα sequence (chimera 11); only slight further activity was obtained by extending the ERα sequences to the middle of H5/6 (chimera 12). Thus, as with PPT, chimera analysis indicated that a considerable portion of ERα sequence is required to support THC agonist activity (Figure 2), including regions that are distal to the ligand binding pocket. However, the ER regions required for the agonistic activity of the two ligands clearly differ. Thus, remarkably, HPTE, PPT, and THC have distinct contributions to ligand positioning that determine their subtype selectivity.

Comparison of Crystal Structures of ERα/β Suggest Amino Acids Involved in Subtype Specificity

An analysis of all published ER crystal structures, as well as molecular modeling of PPT to both ER subtypes (see below), suggests that subtype selectivity derives from a narrowing of the back of the pocket with ERβ, between the β sheet and helices 3 and 6, which force the ligands into alternate binding modes. For THC, this alternate binding mode with ERβ was previously shown to shift H11, forcing H12 into the antagonist conformation (Shiau et al., 2000). A comparison of the amino acids that contact the ligand in 12 published ER crystal structures demonstrates that the β sheet Phe-356/404 (for ERβ/α, respectively) is significantly closer to H3 Glu-305/353 (Student's t test, $T = 3.37$; degrees of freedom $= 11$; $p < 0.001$) and H6 Leu-343/391 ($T = 3.39$; $df = 11$; $p < 0.001$) for ERβ compared to ERα (Figures 5A and 5B). While these differences are too small to be discerned within the limits of resolution of a single structure, the comparison of 12 structures reveals them to be highly statistically significant.

We identified structural features that differ between the ER subtypes and appear to alter the shape of the ligand binding pocket. These amino acids are located at the surface, hydrophobic core, H12, in the β sheet, and H1-H3 coil. Mutations in these respective regions, termed mut-S, mut-C, mut-β, and mut-H1-H3 coil, respectively (Figures 2, 5C, and 5D), were examined for their effects on ligand selectivity, as discussed below.

The altered distance between the β sheet and H3 is associated with a network of surface-exposed hydrogen bonds (Figure 2, mut-S), found only in ERα, that link H3 and the β sheet (Figure 5C), forcing the involved side chains to intercalate between these secondary structural elements and spread them further apart. The coil between H1 and H3 lies between helix 3 and the β sheet and is highly divergent between the ER subtypes (Figure 2, mut H1-H3 coil), suggesting that it may also modulate the distance between the β sheet and H3 (Figure 5C). The hydrophobic core of ER, including amino acids in helices 6, 8, 9, and 11, contains specific differences between ERα and ERβ (Figure 2, mut-C) that appear to alter the distance between H6 and the β sheet (Figure 5D), contributing to the narrowing of the pocket with ERβ. Finally, the strands of the β sheet are significantly further apart in ERβ (data not shown), a feature that may push the β sheet Phe-356 closer to both H3 and H6 (Figure 2, mut-β). This narrowing of the back of the pocket is accommodated differently by PPT and THC, as discussed below.

Molecular Modeling of PPT to ER Subtypes

Molecular modeling suggests that the narrowing of the back of the pocket with ERβ forces PPT to bind in an inverted fashion compared to the binding to ERα. Because we have not yet obtained a crystal structure of PPT bound to either ERα or ERβ, we used molecular modeling to examine what differential interactions might explain its high binding preference (ca. 500-fold) for ERα. Consistent with our earlier phenol deletion/binding affinity studies, we found the C(3)-phenol to be the best mimic for the estradiol A ring (Stauffer et al., 2000), engaging in strong hydrogen bonds with H3 Glu-353 and H6 Arg-394, while the C(5)-phenyl group demonstrated a hydrogen bond with H11 His-524 at the other end of the ligand binding cavity (Figure 5E). The N(1)-phenol forms close van der Waals interactions with H3.

When we placed PPT into the ERβ LBD in the same orientation as in the ERα pocket and performed the docking routine and energy minimizations as before, we were surprised to find that the pyrazole core had flipped over, so that the N(1)-phenol was now on the other side of the cavity (Figure 5E), shifted away from H3. This binding mode eliminated hydrogen bonds with H6 Arg-346 (equivalent to Arg-394 in ERα) and H11 His-475 (equivalent to His-524 in ERα), mimicking the reduced affinities shown by certain mono- and diphenolic pyrazole analogs that also cannot form hydrogen bonds with ER (Stauffer et al., 2000). Thus, the narrowing of the back of the pocket appears to be the structural feature that forces PPT into a low-affinity binding mode with ERβ.

THC Shifts H11 into an Antagonist Conformation with ERβ

For THC, the position of the ligand is different in ERα and ERβ. In the ERβ structure, THC is shifted away from the back of the pocket and toward H11, causing H11 to flex away from the pocket (Supplemental Movie S2, available on *Molecular Cell*'s website; Figure 5A; Shiau et al., 2000). To assess the effect of this flex on the stability of the coactivator binding pocket, ERβ residues in the AF2 region of H3-5 were aligned with the corresponding amino acids in the DES-ERα LBD structure. The position of H11 in ERβ was then compared with the relative positions of helices 11 and 12 in the agonist conformation of DES-ERα. The shift in the backbone of THC-ERβ H11 produces a steric clash with the agonist conformation of H12 that is predicted to force H12 into the antagonist conformation (Figure 5F), an interaction that accounts for the passive antagonism of THC on ERβ. Similar results were obtained when THC-ERβ was aligned with ERα bound to estradiol or THC (data not shown).

This analysis of H11 flexibility suggests that ERβ may also differ in H11 and H12 dynamics. We hypothesize that the agonist conformation of H12 is less stable in ERβ than in ERα and that a preferred localization of H12 away from H11 in ERβ could allow H11 more flexibility. This hypothesis is based on the reduced transcriptional activity of ERβ relative to ERα (McInerney et al., 1998; Sun et al., 1999), the reduced affinity of ERβ for the p160 coactivators compared to ERα (Bramlett et al., 2001; Kraichley et al., 2000), and the structural differences between the two ER subtypes in helices 11 and 12. Specifically, ERα contains a unique salt bridge between the end of helix 12 (Arg-548) and helix 11 (Glu-523) that stabilizes the agonist conformation (Figure 2, Mut-H12). Differences in the hydrophobic packing of the H11-12 loop (Tyr-526, Leu-536) may also contribute to different H12 dynamics. These amino acids, identified as Mut-H12, were introduced into the ERβ construct. Mutations on the LBD surface (mut-S) can also stabilize the agonist conformation of helix 12 by virtue of an ERα-specific hydrogen bond between H3 and H12 (Figure 5C).

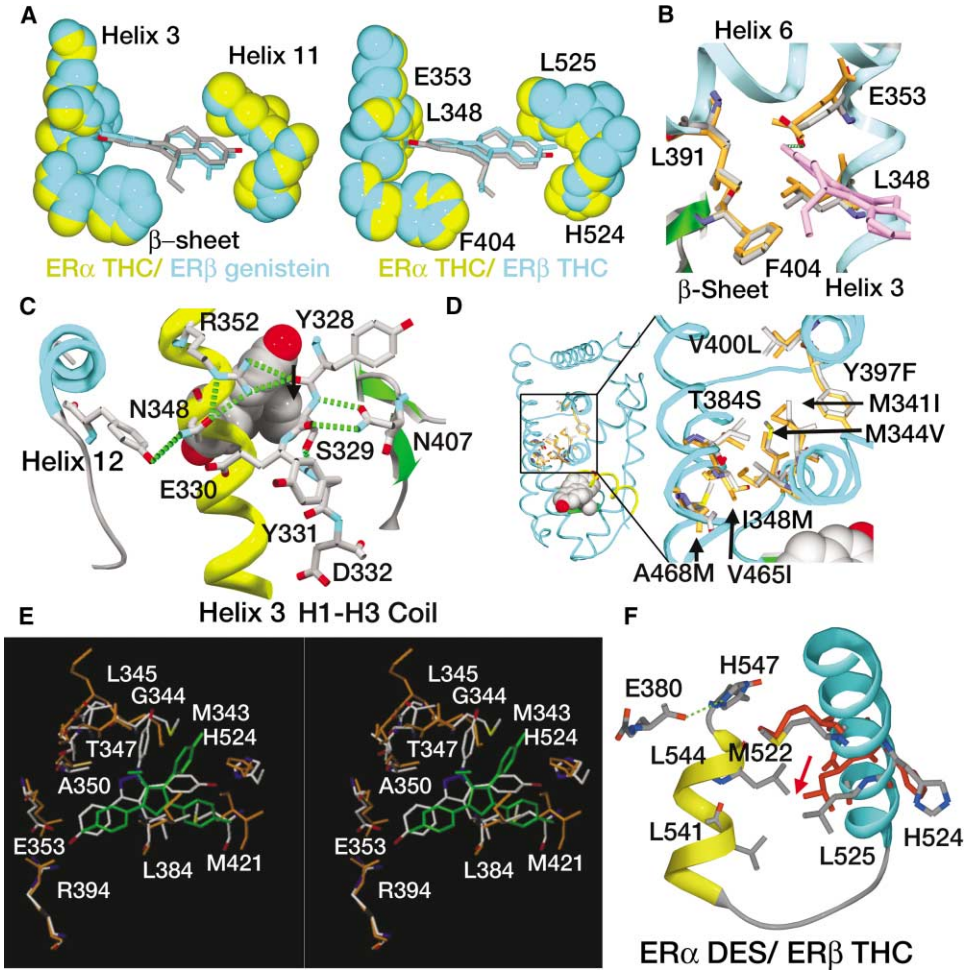

Figure 5. Amino Acids that Control Ligand Orientation for ER Subtypes

(A) ERα (yellow) with THC (gray) was superimposed with ERβ (blue) bound to genistein (left panel) or THC (right panel) using amino acids 307–525 in ERα and the corresponding amino acids in ERβ, excluding any unstructured loops, for an rms deviation of 1.20 Å (genistein) or 0.93 Å (THC).

(B) Portion of the ligand binding pocket of ERα, with THC shown in pink and specified amino acids in gray. The corresponding amino acids in ERβ are shown in orange. Structures were superimposed as in (A).

(C) Ribbon diagram of a portion of the ERαLBD bound to THC (space filled), illustrating a cluster of surface hydrogen bonds specific to ERα, and the H1-H3 coil, which is also highly divergent between the ER subtypes.

(D) Nonconserved hydrophobic core residues clustered around H6 in the ER LBD. The side chains are indicated with the ERβ residue and number, followed by the corresponding ERα residue.

(E) Crossed stereo view of the superposition of the PPT-ERα LBD and PPT-ERβ LBD complexes. Selected residues shown are labeled according to the ERα residues, and portions of some residues are deleted for clarity. PPT in ERα and ERα residues are shown with standard atom colors. PPT in ERβ is shown in green, and ERβ residues are shown in orange.

(F) Superposition of ERβ THC versus ERα DES structures, aligned over amino acids ERα 350–380/ERβ 302–332 for an rms deviation of 0.58 Å. Shown is a ribbon rendering of ERα DES H11 (blue) and H12 (yellow), with amino acids in gray. The corresponding ERβ H11 amino acids are shown in red. Arrows denote predicted clashes between the antagonist ERβ THC conformation of H11 and the agonist ERα DES position of H12. ERβ Leu-476 is 2.5 Å from Leu-544 in H12 of DES-ERα.

Structure-Guided Mutagenesis

Based on the above comparisons, we performed structure-guided mutagenesis of the ERβ LBD to probe the importance of identified amino acid differences in ER subtype-specific selectivity for HPTE, PPT, and THC. While HPTE required only amino acid changes in the ligand binding pocket, PPT needed mutations in the hydrophobic core and surface to gain full agonist activity on ERβ. The recognition of THC as an agonist required all of these mutations, plus those in and around H12. For HPTE, introduction of the two ERα ligand binding pocket residues that differ between the two subtypes into ERβ was sufficient to restore full agonist activity (mut-P, Figures 2 and 6B). The introduction of additional ERα-specific surface residues into ERβ (Figure 5A, mut-P + S) decreased the activity of HPTE, without affecting estradiol activity. Although PPT activity was observed for the mut-P + S ERβ LBD, its potency was well below ERα-mediated activity. A subset of the surface mutations, clustered on H3 [mut-P + S(H3)], yielded a more efficacious response with PPT. This outcome is consistent with the results from the analysis of ERα/β

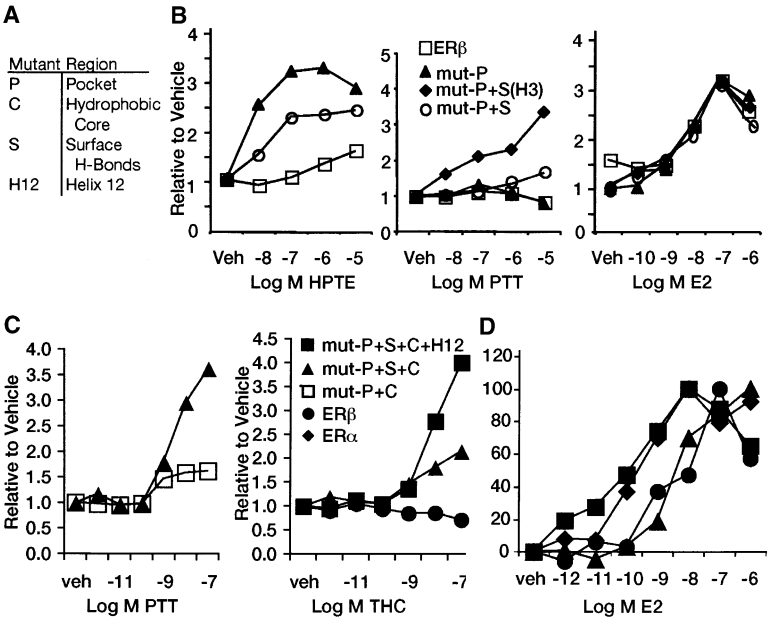

Figure 6. Contribution of Ligand Binding Pocket, Surface, and Hydrophobic Core Amino Acids to Ligand Selectivity

(A) Description of the regions mutated in the various constructs. The amino acids in each cluster are described in Figure 2.

(B and C) Ishikawa cells were transfected with ERβ expression plasmids, the estrogen-responsive luciferase reporter, and the indicated ligands and processed for luciferase activity as described in the Experimental Procedures.

chimeras, in which ERβ sequences in the H3 region appear to modulate PPT potency more so than PPT efficacy. However, none of these ERβ mutations elicited THC agonist activity (data not shown). Notably, the response of all of these mutants to estradiol was identical to that of wild-type ERβ, demonstrating the robustness of this domain with respect to the natural ligand.

Mutation of the cluster of eight hydrophobic core residues in ERβ to the corresponding ERα residues produced statistically significant but still suboptimal agonist activity for PPT when added to the mutations in the pocket (mut-P + C, Figure 6C). The addition of these core mutations to the mut-P + S ERβ produced an ER (mut-P + S + C, Figure 6C) that responded fully to PPT. Since PPT does not bind appreciably to the wild-type ERβ, these data imply that both surface and core mutations contribute separately to ERα binding and agonist potency for PPT. It is noteworthy that seven out of these eight hydrophobic mutations lie within the regions in ERα identified by chimera mapping as being important for specifying the ER subtype preference of PPT, and the eighth is immediately adjacent (Figure 2).

THC differed from PPT in that all of the above-described mutations, including the pocket, hydrophobic core, and surface, were required to elicit any appreciable ERβ agonist activity. The mut-P + C construct displayed no activity. However, THC behaved as an ERβ agonist with the mut-P + S + C construct, although with reduced efficacy compared to ERα (Figure 6C). Since THC binds more avidly to ERβ than to ERα, this change must represent an alteration in the binding mode of THC, an effect requiring both surface and core mutations. Among the eight core mutations, only four are within the region identified through chimera analysis as important for THC selectivity. This difference may relate to the cell lines used, or it may indicate that only these four residues are required.

The addition of H12 mutations to mut-P + S + C ERβ resulted in full THC agonist activity (mut-P + C + S + H12, Figure 6C), although these same H12 mutations had no effect on THC activity when added to the individual mut-P + S or P + C constructs (data not shown). Mutations in the β sheet and the H1-H3 coil were also added to each of the constructs listed in Figure 6. While these latter amino acid clusters appear to contribute to differences in the shape of the ligand binding pocket, they did not alter the behavior of any tested ligand (data not shown).

Surprisingly, estradiol was more active on the mut-P + C + S + H12 ERβ, compared to mut-P + C + S (Figure 6D). This effect required surface (mut-S) as well as H12 mutations, consistent with the observation that these amino acids stabilize the agonist conformation of H12 on ERα. Thus, estradiol was also more potent on mut-P + S + H12 ERβ than on mut-P + S or mut-P + C + H12 ERβ (data not shown).

Role of Helix 11 in Partial Agonist and Dimer-Specific Activity

The above structural and functional analysis of THC selectivity implicates H11 as a key subtype-specific link between the ligand and coactivator binding pockets. To determine the generality of this phenomenon, we examined all of the published NR structures and noted that the conformation of helix 11 was different with partial agonists compared to full agonists and that it varied by dimer partner for PPAR and RXR. While the antagonist THC forces H11 into the space occupied by the agonist position of H12, the three partial agonists shown in Figures 7A–7C allow H11 to flex away from the agonist conformation of H12. This suggests partial agonist activity occurs because of a shift in H11 away from H12 that destabilizes the agonist conformation and the coactivator binding pocket. The structure of RXR bound to the synthetic agonist LG268 (Love et al., 2002) also shows a shift in H11 positioning that may explain its unique behavior. H12 is located away from its agonist position in the LD268:RXR structure, consistent with the reduced

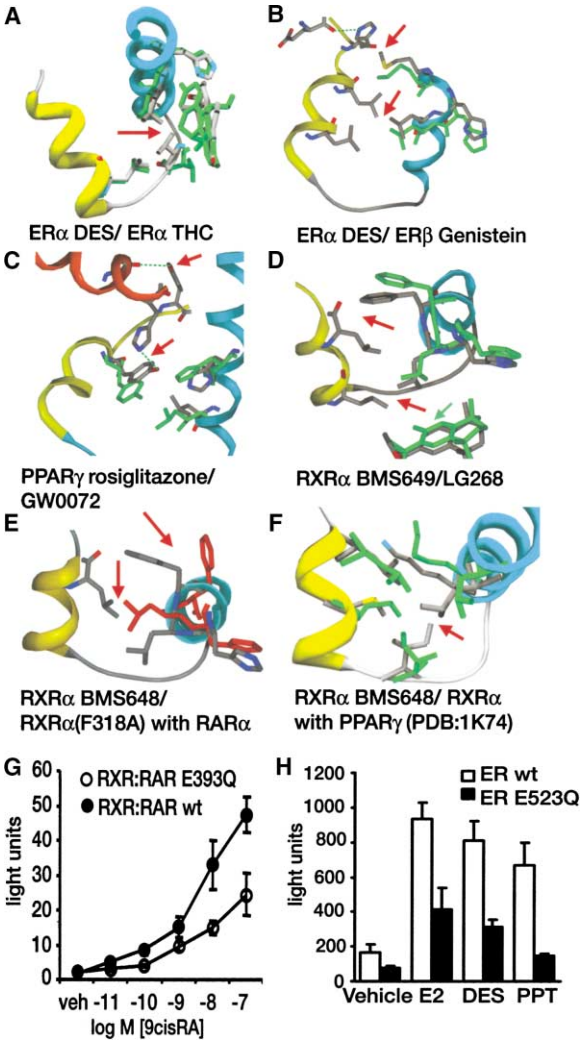

Figure 7. H11 Conformation and the Stabilization of H12

(A–F) An LBD structure with an antagonist or partial agonist was superimposed with a full agonist structure. The full agonist is listed first and shown with the H11 ribbon colored blue and H12 ribbon colored yellow. The agonist amino acids are colored gray. The corresponding H11 amino acids are shown for partial agonists in green or for antagonists in red. Arrows point to predicted loss of VDW contacts or hydrogen bonds or steric clashes with RXR in the heterodimer with RAR, in (E).

(G) A luciferase assay demonstrates effects of mutating the indicated H11 residue located in the dimer interface. COS-7 cells were transfected with RXR and RAR expression vectors and a DR-5 luciferase reporter. Identical results were obtained with all transretinoic acid.

(H) Ishikawa cells were transfected with ERα expression plasmids and an estrogen-responsive luciferase reporter, demonstrating loss of transcriptional activity associated with the H11 mutation. The indicated ligands were used at 10 nM concentration.

displacement of corepressor (Love et al., 2002), limited recruitment of TBP (Lala et al., 1996), and weak activation of RAR:RXR heterodimers relative to other RXR ligands (Germain et al., 2002; Schulman et al., 1997).

Helix 11 position also varies according to dimer partner for RXR and PPAR, demonstrating distinct conformations in heterodimeric structures (Figures 7E and 7F, Supplemental Figures S2A and S2B available on *Molecular Cell*'s website). For RXR, heterodimerization with RAR is associated with inactivation of the RXR AF2 (Bourguet et al., 2000; Westin et al., 1998). In the RAR:RXR heterodimer, helix 11 is flexed into an antagonist conformation (Figure 7E), similar to that seen with THC and ERβ. In contrast, heterodimerization of RXR with PPAR (Figure 7F) elicits a positioning of RXR H11 that resembles the partial agonist conformation. In the PPARγ:RXRα complex (PDB: 1K74, 1FM6, 1MF9) there are 7 $\pm$ 1.1 hydrophobic contacts between RXR H11 and H12, while in the RXRα monomer or homodimers (PDB: 1FBY, 1MVC, 1MZN, 1MV9) there are significantly more contacts (11.2 $\pm$ 1.0, cut off of 4.2 Å; $T = 2.73$; $df = 4$; $p < 0.05$), suggesting that dimer partner influences RXR transcriptional activity by modulating the interaction between H11 and H12. The structural comparisons shown in Figure 7 and Supplemental Figure S2 (available on *Molecular Cell*'s website) were not affected by the choice of full agonist structure, or the precise cut off of the AF2 region used to align the structures.

To test the hypothesis that helix 11 conformation controls AF2 stability and transcription activity, we took advantage of the fact that H11 comprises part of the dimer interface. ER, RAR, and RXR display a conserved Glu amino acid that forms a water-mediated salt bridge across the dimer interface for RXR and ER (Supplemental Figure S2C on *Molecular Cell*'s website), while PPAR contains a Gln at the corresponding position (Gampe et al., 2000), allowing the formation of a hydrogen bond across the dimer interface in the context of the RXR heterodimer (Supplemental Figure S2D on *Molecular Cell*'s website). Conversion of this Glu to Gln or Asn should draw the two H11 closer together across the dimer interface for the RAR:RXR heterodimer, resembling the conformation seen with partial agonist ligands. As shown in Figure 7 and Supplemental Figure S1 (available on *Molecular Cell*'s website), these mutations converted all tested agonist ligands to partial agonists with RAR, RXR, and ER. Notably, the mutant RAR also displayed decreased responses to RXR-specific ligands, LD754 and LD268, and blocked the synergistic effects of combining low doses of RXR- and RAR-specific ligands (Supplemental Figures S1A–S1C on *Molecular Cell*'s website), further supporting the idea that H11 plays a role in transmitting information across the dimer interface. Importantly, the ER and RAR mutants displayed expected dimerization and corepressor associations (Supplemental Figures S1D and S1E on *Molecular Cell*'s website), respectively, demonstrating that the mutant receptors were selectively disrupted in transcriptional activation.

Discussion

Amino Acids Implicated in Estrogen Receptor Subtype Selectivity

Several NR subtypes have been crystallized with subtype-specific ligands, including members of the PPAR, RAR, and TR families, but only residues that make direct contact with ligand have been implicated in the observed specificities. Among the approximately 17 ER LBD pocket residues that contact the ligand, the two residues that differ between ERα and ERβ (L384M,

M421I) are insufficient to explain all of the observed differences in ligand behavior and discrimination. We demonstrate here that residues outside the LBD pocket make significant contributions to the subtype-specific positioning of the ligand. Differences in secondary structural interactions, both in the hydrophobic core of each receptor and in hydrogen bond networks on the surface, alter the shape of the ligand binding pocket between the ER subtypes and the transcriptional output of both receptors. In this way, the link between ligand and coactivator binding is differentially modulated by a few key amino acids distal to the ligand.

Using different cell lines and approaches, our two laboratories independently identified regions of the ER LBD required for ligand selectivity. Importantly, the results were nearly identical. The chimera approach, originally performed in yeast, has the advantage of random selection for gain of function, yet it is not amenable to fine structural analysis. Individual mutations were performed in clustered groups of functional units to maintain hydrogen bonding partners and hydrophobic packing interactions between secondary structural elements. By combining chimera and clustered point mutation data, it is possible to approximate the minimum number of amino acids required for each ligand, while eliminating concerns about loss of binding or gross structural perturbations that can occur with single mutations.

Our observation that mutant ERs respond well to estradiol but variably to other ligands supports the idea that there are "hot spots" for protein folding and mutation (Nikolova et al., 2000) and that most amino acids can be mutated with little effect (Sinha and Nussinov, 2001). We conclude from our data and the data of others that each ligand selects a different subset from the ensemble of conformations. This same principle has allowed the development of therapeutics, such as Gleevec, which selects a unique inactive conformation of the c-ABL protein (Wisniewski et al., 2002), and suggests that similar approaches will work for the NR superfamily.

Allosteric Communication in the Nuclear Receptor Ligand Binding Domain

The transmission of information through structural perturbation is fundamental to the function of many proteins and plays a key role in cellular signal transduction. We have demonstrated that H11 is a conduit of structural information between ligand and H12, though ligand and H12 also interact directly with some receptors, such as PPAR. Both THC/ERβ and RXR in the context of the RAR heterodimer demonstrate a shift in H11 that precludes the agonist position of H12. In contrast, partial agonist activity is associated with a suboptimal conformation of H11 that destabilizes the agonist position of H12 through loss of hydrophobic or electrostatic contacts. This model explains the effects of a glucocorticoid receptor H11 mutation that does not effect ligand binding but reduces coactivator recruitment (Ray et al., 1999; Stevens et al., 2003), presumably through altering the conformation of H11 and destabilizing the active conformation of H12. These effects could be mimicked by a conservative mutation across the H11 dimer interface, converting full agonists to partial agonists for RXR, RAR, and ER and eliminating the synergistic effects of RXR- and RAR-specific ligands without effecting dimerization or corepressor recruitment.

The structural and energetic linkage between the ligand and coactivator binding pockets is demonstrated here to be bidirectional, as mutations effecting H12 contribute to the recognition of THC as agonist or antagonist, presumably through altered binding of the ligand within the pocket. Our structural and functional analyses substantiate a role for the coactivator binding cleft in controlling the positioning of the ligand through the conformation of H11. This concept of bidirectional communication was also demonstrated by the recent crystal structure of PXR, which showed that binding of coactivator elicited an unexpected positioning of the ligand (Watkins et al., 2003).

Our data also suggest that a high-affinity ligand can induce a low-affinity coactivator binding site by selecting for suboptimal conformations of H11 and H12. In addition, the cellular context contributes to the affinity of the ligand because coactivators can stabilize the active conformation, thereby slowing ligand dissociation (Gee et al., 1999). Thus, bidirectional communication between coactivator and ligand can account for discrepancies between ligand affinity and transcriptional potency, as demonstrated with the ER subtypes and estradiol.

Helix 11 flexibility may represent a physiological response that can be co-opted by some ligands, such as THC with ER, to elicit partial agonist (ERα) or full antagonist (ERβ) activity. The natural phyto-estrogen genistein induces a suboptimal conformation of H11 in ERβ compared to estradiol, suggesting that this flexibility is a physiologically relevant response. RXR is another example of this phenomenon, in which the conformation of H11 varies according to NR dimer partner when RXR is bound to its natural ligand, 9-*cis* retinoic acid.

The control of helix 11 conformation by NR dimerization partners also suggests that H11 may contribute to phenomena such as the "phantom ligand effect," in which a ligand bound to one partner alters the activity of the other partner. Thus, the RXR antagonist LD754 can activate the RXR:RAR heterodimer in the absence of RAR ligand (Schulman et al., 1997). Interactions across the H11 dimer interface present a possible structural conduit for communication between dimer partners. Since H11 contacts ligand, H12, and dimer partner, its positioning by a specific ligand could alter the conformation of helix 11 across the dimer interface and, thus, control the binding of both coactivator and ligand in the dimer partner. This model is consistent with the ligand-specific nature of permissive and synergistic activation of RXR heterodimers (Chen et al., 1996; DiRenzo et al., 1997; Forman et al., 1995; Germain et al., 2002; Gupta et al., 2001; Mukherjee et al., 1997).

Experimental Procedures

Chemicals, Materials, and Plasmid Constructions

Cell culture media were purchased from Invitrogen and Gibco BRL (Grand Island, NY). Calf serum was obtained from Hyclone Laboratories (Logan, UT), and fetal calf serum was purchased from Atlanta Biologicals (Atlanta, GA). The luciferase assay system was from Promega (Madison, WI). Plasmids were constructed using standard molecular biology techniques or through PCR-mediated DNA shuf-

fling, as previously described (Sun et al., 2003a, 2003b). RAR and RXR expression vectors and the DR-5 luciferase construct were gifts of Ron Evans. The GST-NCOR construct was a gift of Mitch Lazar. Details of plasmid construction are available upon request. Mutagenesis was performed with the Stratagene Quickchange or Multi-Site Directed Mutagenesis kits. Plasmids were verified by DNA sequencing. HPTE was a gift from Kevin Gaido. The RXR ligands LD268, LD1069, and LD754 were a gift from Ligand Pharmaceuticals.

Cell Culture and Transient Transfections

Human endometrial cancer (HEC-1) cells were maintained in culture as described (Sun et al., 1999). Transfection of HEC-1 cells in 24 well plates used a mixture of 0.35 ml of serum-free improved minimal essential medium and 0.15 ml of Hank's Balanced Salt Solution containing 5 μl of lipofectin (Life Technologies, Rockville, MD), 1.6 μg of transferrin (Sigma, St. Louis, MO), 0.5 μg of pCMVβ (β-galactosidase) as an internal control, 1 μg of the reporter gene plasmid, 100 ng of ER expression vector, and carrier DNA to a total of 3 μg DNA per well. The cells were incubated at 37°C in a 5% CO2 containing incubator for 8 hr. The medium was then replaced with fresh medium containing the desired concentrations of ligands. Reporter gene activity was assayed at 24 hr after ligand addition. Luciferase activity, normalized for the internal control β-galactosidase activity, was assayed as described (Sun et al., 1999).

Ishikawa cells or Cos-7 cells (ATCC) were plated into wells of 48 well plates for transfection. Effectene (Qiagen) was used to transfect Ishikawa cells with 100 ng of TK-ERE-reporter, 5 ng pCMV5-ERα with 20 ng of pBluescript, or 25 ng of pCMV5-ERβ. Cos-7 cells were transfected with Polyfect (Qiagen) and 350 ng of DR-5-luciferase reporter with 25 ng of RARα and 25 ng RXRα expression plasmids. At the time of transfection, cells were switched to media containing charcoal-stripped serum. After 16 hr, cells were washed with phosphate buffered saline and ligands were added. Cos-7 cells were switched to serum-free media upon addition of ligands. After 24 additional hours, cells were lysed for luciferase assay. Data points represent 3–6 separate wells and are representative of at least four experiments.

Structural Analysis

The SwissPDBViewer was used for comparing crystal structures and making figures. Structural superpositions were generated for α carbons based on the following amino acids in H3-5 of the LBD, using a least squares fit method: ERα, amino acids 350–380; RXRα, amino acids 273–303; PPARγ, amino acids 290–320. Other receptor subtypes were aligned using the corresponding amino acids. Figures were rendered with Povray.

Molecular Modeling

The genistein-ERβ LBD crystal structure (Protein Data Bank code 1QKM) (Pike et al., 1999) was imported into SYBYL (Tripos, St. Louis, MO). After adding hydrogen and fixing heavy atoms, energy minimization was performed using the MMFF94 force field. The same procedure was applied to the DES-ERα LBD crystal structure (Protein Data Bank code 3ERD) (Shiau et al., 1998). PPT was built in SYBYL and minimized using the MMFF94 force field. The lowest-energy conformer was docked into the ERβ and ERα LBDs in various orientations. Docking and minimization was done as previously described (Stauffer et al., 2000), and details can be found in that reference. Superposition of the PPT-ERα LBD and PPT-ERβ LBD structures are based on their main chain atoms from H3 to H11, spanning 178 residues (root mean squared difference, 2.15 Å).

Statistical Analysis

Averages are reported as mean ± standard error of the mean. The Student's t test was used for comparing group averages. One factor analysis of variance was used to examine ligand dose effects. Error bars were omitted for clarity on graphs containing overlaid dose curves.

Acknowledgments

We would like to thank Ira Schulman and Robert Fletterick for critical reading of the manuscript; and Andrjez Joachimiak for helpful comments. Ron Evans, Mitch Lazar, and Ligand Pharmaceuticals provided reagents critical to this work. We are grateful for support of this research through grants from the Ludwig Fund for Cancer Research (to G.L.G.) and the National Institutes of Health (P30 CA14599-29 and RO1 CA89489 [to G.L.G.], PHS 5R37 DK 15556 and CA25836 [to J.A.K.], and 5R01 CA18119 [to B.S.K.]). K.W.N. was supported by a D.O.D. predoctoral training grant (BC000661).

Received: August 15, 2003
Revised: January 21, 2004
Accepted: January 23, 2004
Published online: February 5, 2004

References

Bourguet, W., Vivat, V., Wurtz, J.M., Chambon, P., Gronemeyer, H., and Moras, D. (2000). Crystal structure of a heterodimeric complex of RAR and RXR ligand-binding domains. Mol. Cell *5*, 289–298.

Bramlett, K.S., Wu, Y., and Burris, T.P. (2001). Ligands specify coactivator nuclear receptor (NR) box affinity for estrogen receptor subtypes. Mol. Endocrinol. *15*, 909–922.

Chen, J.Y., Clifford, J., Zusi, C., Starrett, J., Tortolani, D., Ostrowski, J., Reczek, P.R., Chambon, P., and Gronemeyer, H. (1996). Two distinct actions of retinoid-receptor ligands. Nature *382*, 819–822.

Darimont, B.D., Wagner, R.L., Apriletti, J.W., Stallcup, M.R., Kushner, P.J., Baxter, J.D., Fletterick, R.J., and Yamamoto, K.R. (1998). Structure and specificity of nuclear receptor-coactivator interactions. Genes Dev. *12*, 3343–3356.

DiRenzo, J., Soderstrom, M., Kurokawa, R., Ogliastro, M.H., Ricote, M., Ingrey, S., Horlein, A., Rosenfeld, M.G., and Glass, C.K. (1997). Peroxisome proliferator-activated receptors and retinoic acid receptors differentially control the interactions of retinoid X receptor heterodimers with ligands, coactivators, and corepressors. Mol. Cell. Biol. *17*, 2166–2176.

Forman, B.M., Umesono, K., Chen, J., and Evans, R.M. (1995). Unique response pathways are established by allosteric interactions among nuclear hormone receptors. Cell *81*, 541–550.

Gaido, K.W., Leonard, L.S., Maness, S.C., Hall, J.M., McDonnell, D.P., Saville, B., and Safe, S. (1999). Differential interaction of the methoxychlor metabolite 2,2-bis-(p-hydroxyphenyl)-1,1,1-trichloroethane with estrogen receptors alpha and beta. Endocrinology *140*, 5746–5753.

Gaido, K.W., Maness, S.C., McDonnell, D.P., Dehal, S.S., Kupfer, D., and Safe, S. (2000). Interaction of methoxychlor and related compounds with estrogen receptor alpha and beta, and androgen receptor: structure-activity studies. Mol. Pharmacol. *58*, 852–858.

Gampe, R.T., Jr., Montana, V.G., Lambert, M.H., Miller, A.B., Bledsoe, R.K., Milburn, M.V., Kliewer, S.A., Willson, T.M., and Xu, H.E. (2000). Asymmetry in the PPARgamma/RXRalpha crystal structure reveals the molecular basis of heterodimerization among nuclear receptors. Mol. Cell *5*, 545–555.

Gee, A.C., Carlson, K.E., Martini, P.G., Katzenellenbogen, B.S., and Katzenellenbogen, J.A. (1999). Coactivator peptides have a differential stabilizing effect on the binding of estrogens and antiestrogens with the estrogen receptor. Mol. Endocrinol. *13*, 1912–1923.

Germain, P., Iyer, J., Zechel, C., and Gronemeyer, H. (2002). Co-regulator recruitment and the mechanism of retinoic acid receptor synergy. Nature *415*, 187–192.

Gupta, R.A., Brockman, J.A., Sarraf, P., Willson, T.M., and DuBois, R.N. (2001). Target genes of peroxisome proliferator-activated receptor gamma in colorectal cancer cells. J. Biol. Chem. *276*, 29681–29687.

Kallenberger, B.C., Love, J.D., Chatterjee, V.K., and Schwabe, J.W. (2003). A dynamic mechanism of nuclear receptor activation and its perturbation in a human disease. Nat. Struct. Biol. *10*, 136–140.

Kraichley, D.M., Sun, J., Katzenellenbogen, J.A., and Katzenellenbogen, B.S. (2000). Conformational changes and coactivator recruitment by novel ligands for estrogen receptor-α and estrogen receptor-β: correlations with biological character and distinct differences

among SRC coactivator family members. Endocrinology *141*, 3534–3545.

Lala, D.S., Mukherjee, R., Schulman, I.G., Koch, S.S., Dardashti, L.J., Nadzan, A.M., Croston, G.E., Evans, R.M., and Heyman, R.A. (1996). Activation of specific RXR heterodimers by an antagonist of RXR homodimers. Nature *383*, 450–453.

Love, J.D., Gooch, J.T., Benko, S., Li, C., Nagy, L., Chatterjee, V.K., Evans, R.M., and Schwabe, J.W. (2002). The structural basis for the specificity of retinoid-X receptor-selective agonists: new insights into the role of helix H12. J. Biol. Chem. *277*, 11385–11391.

McInerney, E.M., Weis, K.E., Sun, J., Mosselman, S., and Katzenellenbogen, B.S. (1998). Transcription activation by the human estrogen receptor subtype beta (ER-beta) studied with ER-beta and ER-alpha receptor chimeras. Endocrinology *139*, 4513–4522.

Meyers, M.J., Sun, J., Carlson, K.E., Katzenellenbogen, B.S., and Katzenellenbogen, J.A. (1999). Estrogen receptor subtype-selective ligands: asymmetric synthesis and biological evaluation of *cis*- and *trans*-5, 11-dialkyl- 5,6,11,12-tetrahydrochrysenes. J. Med. Chem. *42*, 2456–2468.

Mukherjee, R., Davies, P.J., Crombie, D.L., Bischoff, E.D., Cesario, R.M., Jow, L., Hamann, L.G., Boehm, M.F., Mondon, C.E., Nadzan, A.M., et al. (1997). Sensitization of diabetic and obese mice to insulin by retinoid X receptor agonists. Nature *386*, 407–410.

Nikolova, P.V., Wong, K.B., DeDecker, B., Henckel, J., and Fersht, A.R. (2000). Mechanism of rescue of common p53 cancer mutations by second-site suppressor mutations. EMBO J. *19*, 370–378.

Nolte, R.T., Wisely, G.B., Westin, S., Cobb, J.E., Lambert, M.H., Kurokawa, R., Rosenfeld, M.G., Willson, T.M., Glass, C.K., and Milburn, M.V. (1998). Ligand binding and co-activator assembly of the peroxisome proliferator-activated receptor-gamma. Nature *395*, 137–143.

Pike, A.C., Brzozowski, A.M., Hubbard, R.E., Bonn, T., Thorsell, A.G., Engstrom, O., Ljunggren, J., Gustafsson, J., and Carlquist, M. (1999). Structure of the ligand-binding domain of oestrogen receptor beta in the presence of a partial agonist and a full antagonist. EMBO J. *18*, 4608–4618.

Ray, D.W., Suen, C.S., Brass, A., Soden, J., and White, A. (1999). Structure/function of the human glucocorticoid receptor: tyrosine 735 is important for transactivation. Mol. Endocrinol. *13*, 1855–1863.

Schulman, I.G., Juguilon, H., and Evans, R.M. (1996). Activation and repression by nuclear hormone receptors: hormone modulates an equilibrium between active and repressive states. Mol. Cell. Biol. *16*, 3807–3813.

Schulman, I.G., Li, C., Schwabe, J.W., and Evans, R.M. (1997). The phantom ligand effect: allosteric control of transcription by the retinoid X receptor. Genes Dev. *11*, 299–308.

Shiau, A.K., Barstad, D., Loria, P.M., Cheng, L., Kushner, P.J., Agard, D.A., and Greene, G.L. (1998). The structural basis of estrogen receptor/coactivator recognition and the antagonism of this interaction by tamoxifen. Cell *95*, 927–937.

Shiau, A.K., Barstad, D., Radek, J.L., Meyers, M.J., Katzenellenbogen, B.S., Katzenellenbogen, J.A., Agard, D.A., and Greene, G.L. (2000). Structural characterization of an estrogen receptor α agonist/estrogen receptor β antagonist reveals a novel mode of receptor antagonism. Nat. Struct. Biol. *9*, 359–364.

Sinha, N., and Nussinov, R. (2001). Point mutations and sequence variability in proteins: redistributions of preexisting populations. Proc. Natl. Acad. Sci. USA *98*, 3139–3144.

Stauffer, S.R., Coletta, C.J., Tedesco, R., Sun, J., Katzenellenbogen, B.S., and Katzenellenbogen, J.A. (2000). Pyrazole ligands: structure-affinity/activity relationships of estrogen receptor-α selective agonists. J. Med. Chem. *43*, 4934–4947.

Steinmetz, A.C., Renaud, J.P., and Moras, D. (2001). Binding of ligands and activation of transcription by nuclear receptors. Annu. Rev. Biophys. Biomol. Struct. *30*, 329–359.

Stevens, A., Garside, H., Berry, A., Waters, C., White, A., and Ray, D. (2003). Dissociation of steroid receptor coactivator 1 and nuclear receptor corepressor recruitment to the human glucocorticoid receptor by modification of the ligand-receptor interface: the role of tyrosine 735. Mol. Endocrinol. *17*, 845–859.

Sun, J., Meyers, M.J., Fink, B.E., Rajendran, R., Katzenellenbogen, J.A., and Katzenellenbogen, B.S. (1999). Novel ligands that function as selective estrogens or antiestrogens for estrogen receptor-α or estrogen receptor-β. Endocrinology *140*, 800–804.

Sun, J., Baudry, J., Katzenellenbogen, J.A., and Katzenellenbogen, B.S. (2003a). Molecular basis for the subtype discrimination of the estrogen receptor-beta-selective ligand, diarylpropionitrile. Mol. Endocrinol. *17*, 247–258.

Sun, J., Katzenellenbogen, J.A., Zhao, H., and Katzenellenbogen, B.S. (2003b). DNA shuffling method for generating estrogen receptor α and β chimeras in yeast. Biotechniques *34*, 278–288.

Watkins, R., Davis-Searles, P., Lambert, M., and Redinbo, M. (2003). Coactivator binding promotes the specific interaction between ligand and the pregnane X receptor. J. Mol. Biol. *331*, 815–828.

Webb, P., Nguyen, P., and Kushner, P.J. (2003). Differential SERM effects on corepressor binding dictate ERalpha activity in vivo. J. Biol. Chem. *278*, 6912–6920.

Westin, S., Kurokawa, R., Nolte, R.T., Wisely, G.B., McInerney, E.M., Rose, D.W., Milburn, M.V., Rosenfeld, M.G., and Glass, C.K. (1998). Interactions controlling the assembly of nuclear-receptor heterodimers and co-activators. Nature *395*, 199–202.

Wisniewski, D., Lambek, C.L., Liu, C., Strife, A., Veach, D.R., Nagar, B., Young, M.A., Schindler, T., Bornmann, W.G., Bertino, J.R., et al. (2002). Characterization of potent inhibitors of the Bcr-Abl and the c-kit receptor tyrosine kinases. Cancer Res. *62*, 4244–4255.